

Chapter 1

Targeted Selection and Characterisation of Contemporary HTS Wires for Specific Applications



Stuart C. Wimbush

1.1 Present Status of Large-Scale Applications of HTS

Large-scale HTS applications have now been successfully demonstrated in almost every proposed sphere [1]: e.g., motors [2], fault current limiters [3], power cables [4], maglev trains [5], magnetic [6] and flywheel [7] energy storage systems, transformers [8], wind generators [9], research (beamline [10] and high-field [11]) magnets, magnetic resonance imaging [12] and nuclear magnetic resonance [13] devices. About the only outstanding application that has yet to be demonstrated is the fusion reactor, and here too device construction and testing is already underway [14, 15]. The field of applied, technological superconductivity is now moving beyond these preliminary demonstrators to the industrial development of commercially viable machines and devices. At this stage, it is no longer proof of concept that governs conception but rather proof of viability. New drivers emerge such as cost-effectiveness, reliability, practicality and competitiveness with incumbent technologies.

At the same time, the number of commercial HTS wire manufacturers active in the industry has grown quite considerably in recent years and continues to grow. Whereas in the past, choice was limited to three or four established manufacturers, often operating at capacity, now there are a dozen advertising the ability to supply significant quantities of wire on a commercial basis, with a similar number in a pre-production ramp-up phase. It must be said, however, that total production capacity remains well below projected demand, meaning that supply issues continue to play a role.

S. C. Wimbush (✉)

The Robinson Research Institute of Victoria University of Wellington, Wellington, New Zealand
e-mail: stuart.wimbush@vuw.ac.nz

In this context, a new requirement arises, which is for the informed and targeted selection of appropriate wire for a given project in the face of a broad selection of widely varying and poorly specified material combined with uncertainty of supply. Where a significant investment decision is to be made on the open market, rather than a particular wire supplier being pre-specified under the terms of a joint research programme, the need to confirm that performance requirements will be satisfied and to secure the optimum economic outcome becomes an important task in the project. Even for a relatively small build of any practical device, wire cost at present prices constitutes a significant fraction of the total build cost so the saving to be made by not over-specifying the wire cannot be overlooked, and indeed may make the difference in viability of the project as a whole. This chapter examines the benefits of detailed project-specific wire characterisation, and the opportunities that targeted wire selection offers to improve the efficiency and economy of device designs.

1.2 Wire Characterisation Systems

The requirement outlined above for more detailed wire characterisation than is commonly provided by suppliers at this time in terms of the critical current, I_c , under different conditions of temperature, magnetic field and field angle, targeting the specific application, has begun to be recognised [16, 17]. The high performance of contemporary HTS wires presents a particular challenge due to the multiple kiloamps of current now needed to adequately characterise full wires under the conditions of interest for many applications. The majority of characterisation systems described in the literature [18–21] continue to rely on liquid helium for their operation; however, this limits both their speed of operation and their ultimate cost effectiveness, with even the best-designed systems [20] consuming upwards of 0.5 l of liquid helium per I_c data point acquired.

At the Robinson Research Institute, we have developed and refined our own in-house HTS wire critical current measurement system [22], shown in Fig. 1.1, over a period of several years. Our system relies on a cryocooled 8 T split-pair HTS magnet to provide a horizontal magnetic field within which out-of-plane sample rotation is relatively easily accomplished whilst accommodating the hefty current leads required to convey kiloamps of current to the sample without excessive heating. A circulating cryocooled helium gas sample cooling circuit likewise provides continuous liquid cryogen free operation down to a base temperature (with sample and current leads inserted) presently around 12 K. Full automation of the measurement routine allows for long but efficient characterisation runs generating upwards of 100 distinct IV curve measurements per hour, with automatic determination of I_c and n -value at each point. Sample exchange can conveniently be performed while the system remains cold and is typically completed within 30 min, opening the possibility of high-throughput characterisation of many wire segments under more highly targeted (but still application-relevant) conditions.

Fig. 1.1 The Robinson Research Institute's SuperCurrent I_c measurement system enables the automated electrical characterisation of full HTS wires at temperatures down to 15 K, magnetic fields up to 8 T, and currents up to 1 kA. Complete 360° rotation of the sample within the magnetic field allows detailed characterisation of the wire anisotropy in addition to the more common temperature and field dependences of the critical current



All of the experimental data presented here was acquired on this system, and much of it is available to download freely from our publicly accessible HTS wire database [23] located at <https://www.victoria.ac.nz/robinson/hts-wire-database>. By making this exemplary data widely available, it is our intention to encourage superconducting device designers to investigate how their designs could be modified to operate more efficiently on the basis of the availability of this information, and in the remainder of this chapter, we address some of the approaches successfully employed to achieve this, illustrated by a number of case studies highlighting specific aspects of the actual device design process.

1.3 Wire Characterisation Under Different Regimes

Understanding the behaviour of different wires under different regimes of operating parameters is central to the efficient design of superconducting devices, with the range of variation across commercially available materials being extremely large and different wires being optimised in often only partially understood ways for different nominal applications that may not tally particularly well with actual real-

world conditions. The primary operating conditions of relevance to superconducting materials are the temperature and the magnetic field. Due to the inherent anisotropy of the HTS materials, as well as the intentional introduction of microstructural defects aimed at enhancing performance through improved flux pinning, the direction of the magnetic field relative to the crystal structure of the superconductor is also an essential parameter, often equally as significant as its magnitude. Each of these parameters—temperature, magnetic field and field angle—will be addressed in turn.

1.3.1 Temperature Regime

The most basic question to be asked of any potential application is its intended temperature of operation. If a device is to operate immersed in an open bath of liquid nitrogen then this fixes this parameter at the most commonly reported temperature of 77 K. In practice, this arrangement would be rare for a practical device, however. More common is that the application must be considered to exist across a range of temperatures, for example in the transition from cryogenic to room temperature in the gas above the bath, or in the case of sub-cooled liquid nitrogen in the temperature range from the nitrogen triple point of 63 K at the coolest part of the bath to 77 K at its warmest. Even an open liquid nitrogen bath will vary in temperature by up to a few degrees depending on the ambient air pressure (and therefore altitude).

Where an electrical cryocooler is to be used, the situation may be turned on its head, with the operating temperature being dictated instead by the requirements of the application, and an appropriately powered cryocooler being specified on this basis. In this situation also, it is appropriate to speak of a range of temperatures, since in powered (rather than passive) applications, accommodations must be made for the varying load on the cryocooler, and in practical terms also for the variation in cryocooler performance between maintenance periods.

The establishment of the intended operating temperature regime is a crucial first step in the decision-making process regarding wire selection, immediately demarcating a number of broad boundaries. Common choices include 77 K liquid nitrogen, 65 K sub-cooled liquid nitrogen, 30 K cryocooled, 10 K cryocooled and 4.2 K liquid helium, but the choices are essentially limitless, to be dictated by the other design constraints imposed on the application.

It is now well established, nor is it surprising given the complexity of the flux pinning process that ultimately governs the wire I_c as well as the vast range of advanced processing techniques employed in wire manufacture, that it is impossible to predict purely on the basis of, for example, 77 K performance, what the performance of a particular 2G HTS wire will be at a distant temperature, for example 30 K, and that even extrapolations over relatively limited temperature ranges from 77 K to 65 K are fraught. The most immediate example of this has been presented in [24], where two wire samples are compared, one of which performs

better at 77 K and the other at 20 K. In light of the potential for such a reversal in relative performance, it is evident that given no knowledge of a wire other than its 77 K performance, no reliable prediction can be made of its performance at another temperature, or under a given magnetic field. It is important to recognise that where such correlations have been demonstrated to exist [25], these have been between pairs of carefully selected temperature/field combinations at a single field orientation and amongst samples of a highly similar nature, for example identically prepared materials differing only in degree of chemical doping. No such correlation is generally applicable, nor could it ever be.

The reason for this is clear: the wire performance is determined by the flux pinning effectiveness, and different pinning centres have strengths that vary in dependence upon the temperature and magnetic field in different ways. It will only ever, therefore, be possible to correlate wire performance across temperatures in samples that possess the same population of pinning defects (both controlled and uncontrolled), and this is what is seen in practice. For a reliable evaluation of the performance of an arbitrary sample, there is simply no alternative to measuring its performance within the proposed operating temperature regime (see **Case Study: Traction Transformer**).

An inadequately resolved matter confronting the research community at the present time is the identification and implementation of an effective low-temperature pinning defect. All of the most prominent pinning centres, for example BaZrO_3 nano-columns, lose their effectiveness at low temperatures [26]. Is this merely a result of the relative ease with which experimental investigations can be performed at 77 K encouraging greater empirical effort in this regime, is it that pre-existing natural sources of pinning become stronger at low temperatures as vortices stiffen, obscuring attempts to further strengthen the pinning force, or is there a fundamental lack of effective low-temperature pinning structures? The answers to these questions are presently unclear.

To date, the most promising route to low-temperature performance enhancement has been using the method of ion irradiation to create flux pinning damage track defects running through the material [26, 27]. The direct applicability of this method to industrial production is questionable, but not to be ruled out [28]. Most likely, an improved understanding of low-temperature flux pinning processes is required to be derived from such studies, before more practical processing techniques can be developed to generate the appropriate defect structures in a more facile manner.

Case Study: Traction Transformer

The development of superconducting transformers for use on trains offers the particular advantage of reduced component weight, in addition to the increased efficiency and reduced fire risk that is of benefit to all types of

(continued)

superconducting transformers. A transformer is an inherently AC device, and consequently the design of any practical superconducting transformer is centred on the management of AC loss. If the aim is to achieve an efficiency target of 99% in a transformer that may have a power rating of 6.5 MVA, for example, then it is immediately apparent upon taking into account a realistic cooling penalty (ratio of cooling power required at room temperature to extract a given amount of heat at low temperature) of ~ 15 at 65–77 K that the total losses (AC loss plus thermal load due to current leads, etc.) cannot be allowed to exceed 4 kW. Furthermore, not only the transformer unit itself, but also its associated cooling system must meet the stringent design limitations of overall size and weight. At the same time, in contrast to the high-field electromagnets that form the core of many superconducting devices, the magnetic fields experienced by the superconductor in this application lie squarely at the low end of the scale, unlikely to exceed about 0.5 T. Given the low field requirement in combination with the intrinsically mobile nature of the application, a cooling system based on liquid nitrogen or operating at the higher end of the temperature scale in order to minimise the cooling penalty and reduce the complexity of the cooling system is most practicable.

A survey of the temperature-dependent performance of commercial wires available in the quantity (~ 15 km) required to accomplish the build (Fig. 1.2)

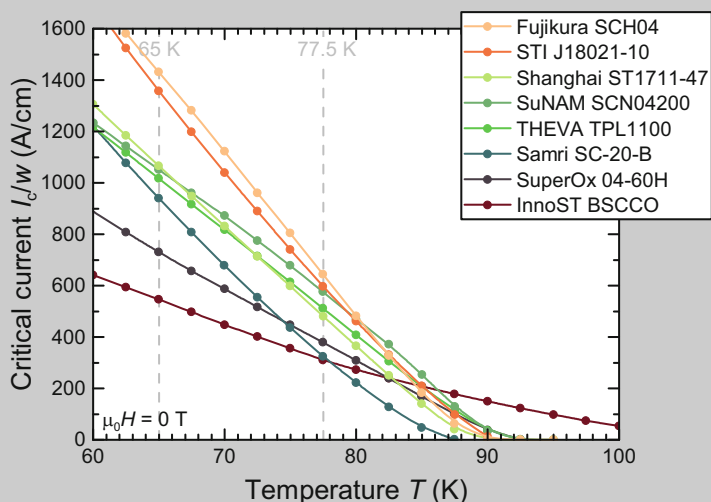


Fig. 1.2 Self-field temperature-dependent performance comparison of commercial HTS wires sourced from various manufacturers in the sub-cooled liquid nitrogen temperature range, highlighting that in general different wires may perform better at 65 K than those that perform best at 77 K

(continued)

indicated that even the best available wires provided insufficient performance to operate at 77 K, and so an operating environment of sub-cooled liquid nitrogen extending down to 65 K was adopted. It is notable that even this relatively small variation in operating temperature already introduces a different ranking to the relative performance of the wires than would be obtained at the commonly specified temperature of 77 K.

To further qualify the potential wires for this application, and to facilitate detailed and accurate modelling of the AC loss critical to successful operation of the device, the full angle dependence of the critical current of each wire under consideration was determined at fine intervals throughout the relevant field range from 0 T to 0.5 T, with a particular focus on fields below 0.2 T where in particular, the in-plane performance of the wires varies rapidly. From these full angle dependencies were extracted the minimum and maximum I_c values at each field, as shown for the intended operating temperature of 65 K in Fig. 1.3. In most cases, these minimum and maximum I_c values correspond with those obtained for fields oriented parallel and perpendicular to the wire direction, respectively, but in some cases, there were significant deviations (see Sect. 1.3.3).

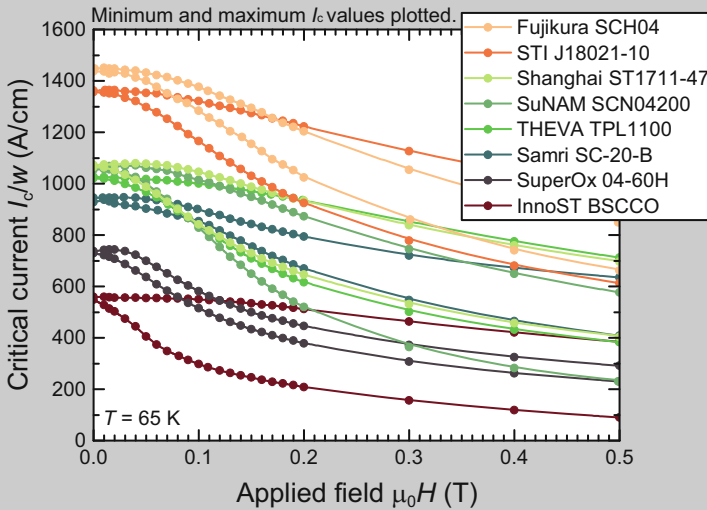


Fig. 1.3 Low-field performance comparison of available commercial HTS wires sourced from various manufacturers at the temperature of sub-cooled liquid nitrogen (65 K). Minimum and maximum I_c values extracted from full angle dependencies under each condition are plotted in order to encompass the full range of performance at each field value

(continued)

As detailed in Sect. 1.3.2, careful examination of the behaviour of widely available superconducting wires in the low-field regime reveals a large array of hitherto underexplored features and subtleties that should be taken into account in any data-based design.

On the basis of this data, we conclude that Fujikura and STI wires offer a level of performance under the conditions of relevance to this application that lies significantly ahead of other contenders. A number of other suppliers then occupy the mid-range, although here the situation is not so clear-cut since the critical region of the transformer is going to be at the end turns of the windings, where significant out-of-plane fields will impinge on the wire, and the performance of some of the wires under these conditions is seen to be poorer in spite of better performance overall.

Ultimately, a full numerical model serves to indicate whether a given wire performance is adequate to realise successful operation of the device, and from there an economic decision can guide the purchasing choice.

1.3.2 *Field Regime*

A relatively common form of wire characterisation is the field dependence of I_c measured at a particular temperature (most commonly 77 K), usually for fields applied both perpendicular and parallel to the plane of the tape (Fig. 1.4). This is the sort of product data that the more established wire manufacturers typically provide (for a good example, see [30]). The choice of the two orthogonal field orientations is based on the supposition that these provide some measure of extreme (minimum and maximum) values, but this is a hangover from the specific case of 1G (BSCCO) wire, where it can broadly be relied upon to be true [31]. In the case of 2G (REBCO) wire, this supposition, unchecked, can be highly misleading as will be evidenced in Sect. 1.3.3. In particular, the perpendicular field I_c , initially observed to represent the minimum value, has over time become a metric for performance enhancement through the introduction of artificial pinning centres, but the consequent focus on enhancements in this specific field direction has tended to overlook the fact that the minimum I_c has shifted elsewhere, and that little usable performance enhancement may actually have been achieved (see Fig. 1.5). Instead, it can be preferable in the case where a visual overview of comparative wire performance is required to plot the true minimum and maximum values (as shown, for example, on Fig. 1.3), although this does typically require the measurement of the full angular dependence of I_c under each condition to reliably determine, and it runs the risk of introducing its own overestimations of performance if it is subsequently assumed that the minimum occurs for fields applied in the perpendicular direction, and that the I_c experienced when fields are oriented in other directions will be higher.

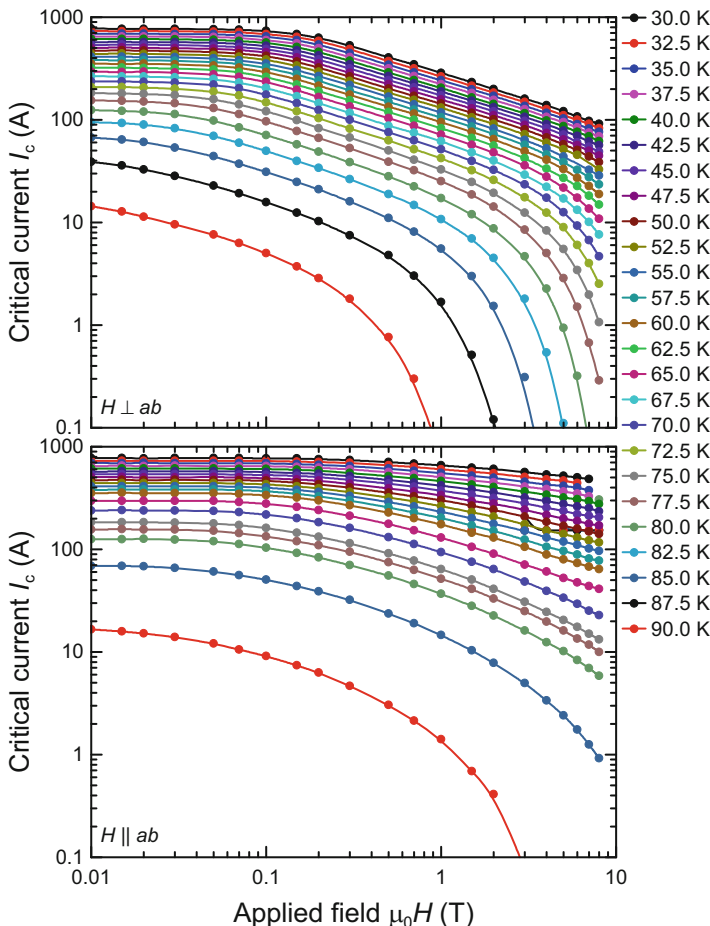


Fig. 1.4 Field dependence of the critical current of a SuperOx 2G HTS wire sample over a range of temperatures (lowest temperature corresponding to highest I_c) for fields applied perpendicular (upper panel) and parallel (lower panel) to the plane of the wire. A pronounced sensitivity to out-of-plane fields is evident on this double logarithmic scale, common to most 2G wires. Data from [29]

Out-of-Plane Field Hysteresis

The basic behaviour exhibited by the field dependences is that as the field is increased, and correspondingly the number of flux vortices present within the superconductor increases, the strongest available pinning sites become occupied and successively weaker pinning sites begin to be populated, leading to a reduction in I_c to higher fields until the irreversibility field is reached and I_c drops to zero. At the lowest fields and lower temperatures, grain boundary derived limitation of the superconducting cross-section may dominate the behaviour, resulting in a plateau region of constant I_c [33].

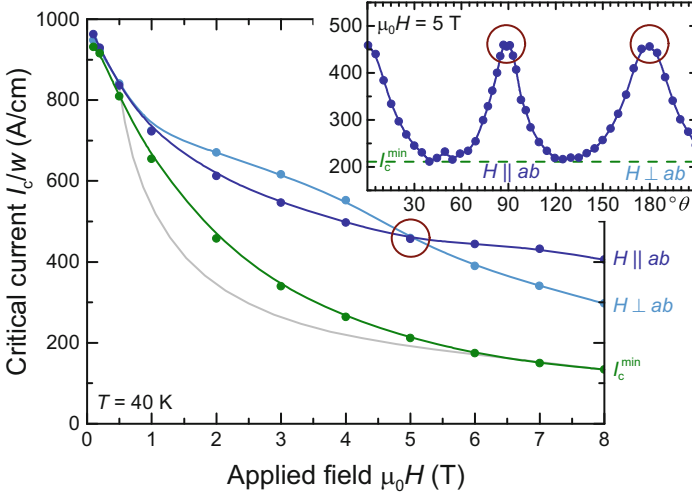
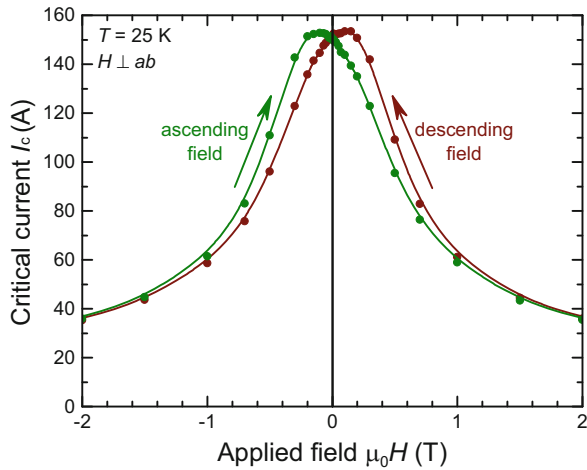


Fig. 1.5 Field dependence of the critical current of an American Superconductor 2G HTS wire insert with strongly enhanced c -axis pinning introduced via ion irradiation, highlighting how a focus on parallel and perpendicular field behaviour can obscure the true envelope of performance of the wire as accurately represented by the minimum I_c value. The grey curve indicates the original (unirradiated) minimum I_c , showing the true extent of the performance enhancement due to irradiation. The angle dependence of I_c (inset) under the highlighted condition shows how the situation of apparent isotropy can arise in the case of pinning-enhanced material. After [32]

Fig. 1.6 The field dependence of I_c at low temperatures exhibits hysteresis at low fields depending on the direction of the field sweep as flux vortices get trapped within the grains such that the field in the grain boundaries (which limits I_c) reaches zero before the applied field. Where only a single non-virgin field quadrant is swept, this can lead to an underestimation of the true zero field I_c , or a spurious peak effect



When we examine the field-dependent I_c for fields applied perpendicular to the wire in both the increasing and decreasing sense (Fig. 1.6), we observe a hysteretic behaviour at low fields (typically less than 1 T). The maximum I_c value is seen not to occur at zero applied field, but rather to occur *before* zero field is reached (in

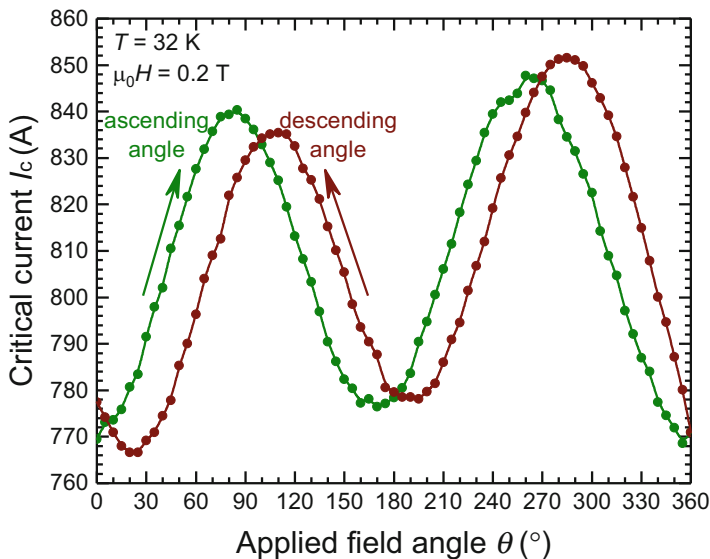


Fig. 1.7 The angle dependence of I_c at low temperatures is shifted in angle at low fields due to field trapping within the grains

whichever direction the field is being swept). This effect has been well documented in granular materials [34] and in films containing engineered large-angle grain boundaries [35], and it is found to be ubiquitous in coated conductors due to their inherent grain boundary network [36]. The proposed explanation is that the field (comprising flux vortices) becomes trapped within the grains, causing the grain boundaries to reach zero localised field before the applied field reaches zero. Since it is the grain boundaries that limit I_c in the low-field regime, this reduced grain boundary field is immediately reflected in the measured I_c .

Less commonly observed [37] is that this out-of-plane field hysteresis carries through also to the angle dependences of I_c , where the offset between the results obtained with increasing and decreasing field angle can be rather large, as much as 30° (Fig. 1.7). Again it is observed most strongly at low fields and low temperatures, and as with the field hysteresis, the angular peaks in I_c are observed to occur “too soon.” To get an accurate measure of the correct angular location of the curve, there is no option but to measure in both directions and then to shift the curves equally into alignment, or to measure each point after zero field cooling at that angle. Otherwise, the true angular position of the curve must be inferred.

In-Plane Field Asymmetry

A well-reported effect in 2G wires [38] is the asymmetry of the field dependence of the critical current to positive and negative in-plane fields, attributed to the

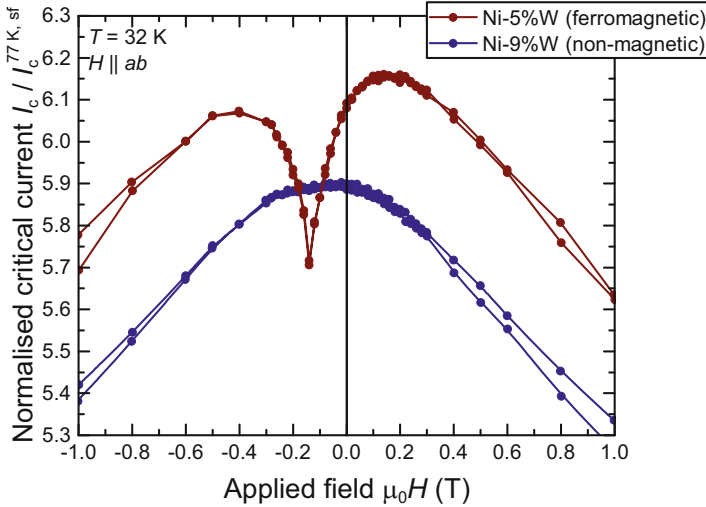


Fig. 1.8 Asymmetry about zero field in the in-plane field dependence of I_c at low fields caused by differing surface barriers to vortex motion, and additional general enhancement and localised suppression of I_c at non-zero field caused by the presence of a ferromagnetic substrate. Note that no hysteresis is observed in these in-plane measurements. I_c is plotted normalised to allow direct comparison of the two effects since the wires on different substrates have different I_c . After [39]

difference between the surface barriers to vortex motion at the interface between superconductor and dielectric buffer layers on one hand, and superconductor and metallic capping layer on the other. Since reversal of the field direction reverses the direction of the Lorentz force acting on the vortices, they encounter one or other of these surface barriers, leading to a different I_c (for small fields). Reversal of the current direction is confirmed to produce the same effect.

A recently reported extension of this observation [39] highlights the additional, superimposed effect of a sharply reduced dip in I_c over a narrow, non-zero field range in the presence of a ferromagnetic substrate (such as the Ni-5%W alloy commonly used in the RABiTS process), reproduced in Fig. 1.8. Again, the effect was confirmed to reverse in field in case of reversal of the current transport direction, or if the sample was placed face-up instead of face-down (reversing the direction of the Lorentz force relative to the wire). Furthermore, exfoliation of the sample from the magnetic substrate was demonstrated to eliminate the dip in I_c , while sandwiching the sample between two Ni-5%W foils was seen to produce a double dip to either side of zero field. Finite element modelling shows the effect to be the result of field shaping by the ferromagnetic substrate causing a significant perpendicular field component to be generated within the wire by the self-field resulting from the transport current even though the applied field lies strictly within the plane. A notable side-effect of this field shaping is a reduction in the overall field seen by the superconductor, resulting in a general enhancement of I_c [40].

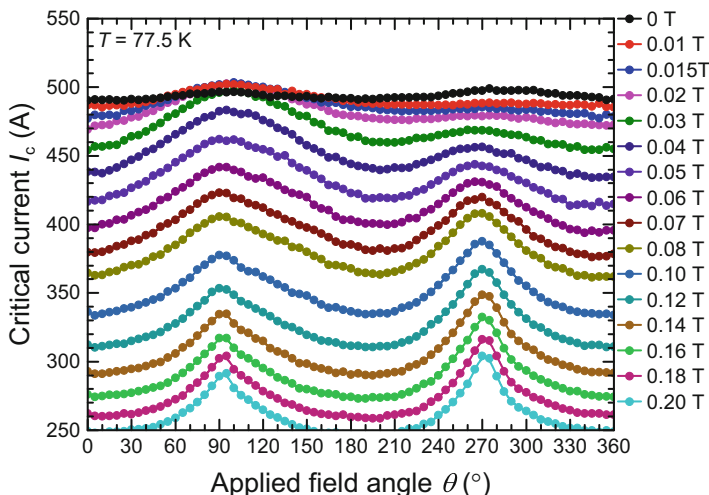


Fig. 1.9 The in-plane (90°) peak in the angle dependence of I_c of a Fujikura 2G HTS wire sample at low fields exceeds the zero-field value due to the in-plane field asymmetry highlighted in Fig. 1.8. The peak for fields applied in the opposite (270°) direction is correspondingly diminished

The consequence of these effects is an apparent irregularity and the loss of 180° periodicity in the angle dependence of I_c of these materials at low fields, and in particular at low temperatures (where the I_c is high). The effect also gives rise to a characteristic peak in the angle dependence at low fields that exceeds the zero-field I_c value (see Fig. 1.9). This particular combination of conditions is not a common one for present applications, but the effect is present to a lesser degree at higher temperatures also, as Fig. 1.9 demonstrates, so it may be important to take into account in any low-field application such as power cables, transformers or fault current limiters.

Case Study: Wind Power Generator

A prototype HTS wind power generator was designed and constructed at the 10 kW scale [41], in part to test the use of a brushless exciter to energise the HTS rotor coils in a non-contact manner through the walls of the rotating cryostat [42]. Although the design was informed by measurements of the performance of the HTS wire used in its construction, the paucity of available wire data from different suppliers meant that it was not possible to select wire specifically targeted to this application.

(continued)

Table 1.1 Comparison of the constructed design for a 10 kW HTS wind power generator with a refined design utilising data for an optimally selected alternative wire

		Original design	Refined design
Design specifications	Rated output power	10.3 kW	
	Rotational speed	300 rpm	
	Operating temperature	30 K	
HTS rotor coil design	Width of racetrack coil bobbin	25 mm	
	Total width of racetrack coil	95.5 mm	68.5 mm
	Effective length of racetrack coil	170 mm	200 mm
	Turns of HTS per coil	235	145
	Operating current	91 A	336 A
	Current margin	40% below I_c	
	Number of poles	6	
	Number of coil layers per pole	4 (QPC)	2 (DPC)
	Total length of HTS wire required	3 km	1 km
	Results	Inductance	0.15 H
Overall diameter of the generator		453.3 mm	183.5 mm
Maximum magnetic field on coil		2.2 T	5.8 T
Max. perpendicular magnetic field		1.1 T	2 T

Original design from [41]; refinement calculation courtesy of H.-J. Sung

Post-construction, it was of interest to run the design model using a range of datasets of alternative wires that could have been used had this data been available. Table 1.1 highlights the design modifications and the resulting benefits that could potentially have been realised in the best case.

By selecting the best available wire for the specific operating conditions of the target application (30 K, reduced sensitivity to perpendicular fields), it would have been possible to increase the operating current significantly whilst maintaining the safety margin to I_c , optimally balancing the field on the coils against the operating current to minimise the coil size, and ultimately reducing the amount of wire required for construction from 3 km to 1 km at the same time as halving the overall build diameter of the generator. It is likely that under an economic analysis, these benefits would outweigh any additional cost associated with the superior wire. A fully detailed wire characterisation is also likely to increase confidence in the actual wire performance, enabling a reduction in the operating current margin and consequent further design gains.

1.3.3 Angular Regime

The full power of detailed wire characterisation is realised when complete angle-dependent variations in I_c are measured and utilised in device designs. Combined with numerical models able to account for the full wire anisotropy, great improvements in the efficiency of wire utilisation can be achieved (see [Case Study: MRI Magnet](#)) as we move from designs based on the anticipated minimum I_c of the wire for a given field–temperature combination to designs able to fully utilise the performance benefit available from HTS wires in regions of partial in-plane field.

This potential performance gain is exemplified in the data shown in Fig. 1.10, where it is seen that for a relatively wide angular range around the in-plane

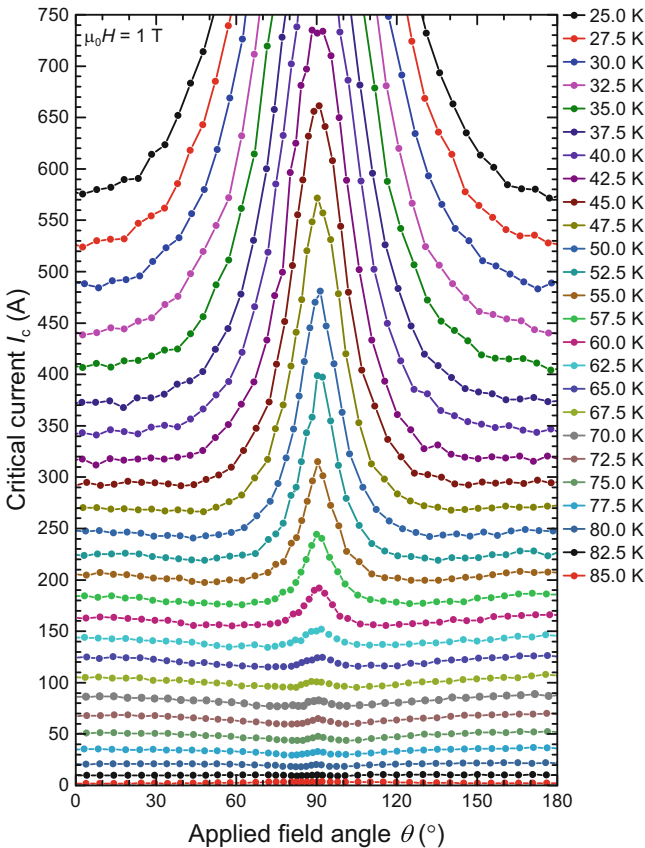


Fig. 1.10 Angle dependence of the critical current of an American Superconductor 2G HTS wire sample over a range of temperatures (lowest temperature corresponding to highest I_c) at an applied field of 1 T. The performance gain available when the field is aligned close to the in-plane (90°) direction is evident at low temperatures, as is the fact that to higher temperatures as the peak narrows the true I_c minimum is not located at 0° but closer to the base of the peak, even for this non artificially pinning-enhanced wire. Data from [43]

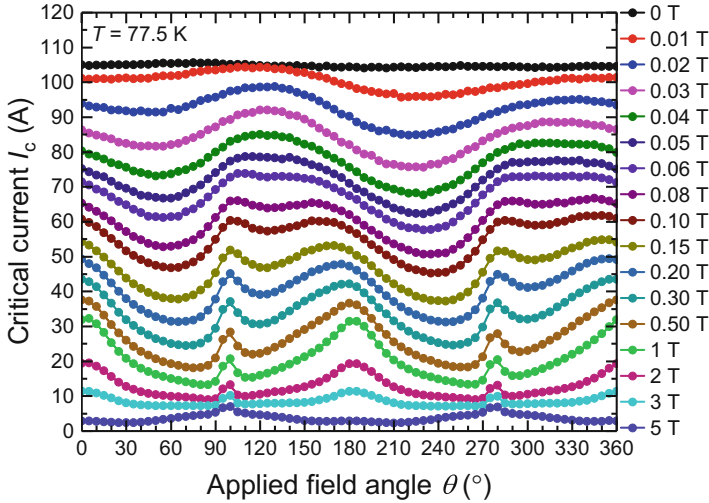


Fig. 1.11 Full 360° angle dependence of the critical current of a SuperPower AP 2G HTS wire sample over a range of applied magnetic fields (lowest field corresponding to highest I_c), showing a high degree of asymmetry about the in-plane (90°) peak at high temperature, low field, due to the addition of correlated pinning centres aligned with the perpendicular direction. Towards higher fields, this asymmetry is reduced and then eliminated concurrently with the suppression of the out-of-plane (180°) peak as these artificial pinning centres become ineffective. A further, more subtle, asymmetry between half-revolutions is also seen to evolve, with I_c values in the second half cycle being slightly lower at low fields, then rising to slightly higher values at fields around 0.1 T, before equalising at higher fields. This same effect is also seen in the earlier, non pinning-enhanced, data of Fig. 1.9

field direction, particularly at low temperatures, significantly higher I_c values are available to utilise than the minimum I_c approximated by the out-of-plane value. This dataset also serves to highlight that even in 2G wires with a relatively simple angular behaviour and an absence of intentionally added artificial pinning centres, the true I_c minimum is not necessarily obtained for fields applied perpendicular to the plane of the wire, but can be located closer to the base of the in-plane peak. A much more complex (and more common) example of the angular anisotropy of I_c in the presence of artificial pinning centres will be shown in the next section (Fig. 1.11).

Wire Asymmetry

Detailed studies of pinning-enhanced wires under conditions of high temperature and low field reveal a surprising degree of asymmetry in the angular dependence of I_c about the in-plane direction (Fig. 1.11). The I_c to one side of the in-plane pinning peak can be significantly (up to 30%) greater than to the other side. This raises the

prospect of some clever engineering being applied to utilise this potential benefit, by paying careful attention to the wire orientation when winding a coil.

Hybrid coils using 1G wire in the central windings (where the field is predominantly parallel to the plane of the wire) and 2G wire in the end windings (where the field diverges towards the perpendicular direction) have been investigated [44]. However, the present data highlights the importance of carefully controlling the orientation of the 2G end coils to ensure that the direction of divergence of the field matches the orientation of best performance. In this manner, a significant overall performance gain can be expected [45].

Also of note in the data of Fig. 1.11 is the extreme repositioning of the minimum I_c value much closer to the base of the in-plane peak than to the perpendicular direction. A relatively small deviation in field direction of $\pm 30^\circ$ from in-plane takes the wire all the way from its maximum I_c to its minimum I_c , although as highlighted above this minimum I_c may be significantly different to either side of the peak. As discussed in Sect. 1.3.2, using the perpendicular I_c as an inaccurate estimate of the minimum I_c in this case would overestimate the true value by up to a factor two.

A particularly striking example of wire asymmetry under all operational conditions arises in the case of films textured via the method of inclined substrate deposition (ISD) [46], as shown on Fig. 1.12. Here, due to the growth mode, the crystal structure of the superconductor is not aligned with the coordinate system of the wire. In contrast to the more commonly employed ion beam assisted deposition (IBAD) method of texturing, where an inclination of up to a few degrees is common (see offset of the in-plane peak to the right of 90° at high fields on Fig. 1.11), or the RABiTS textured substrate which produces film growth exactly perpendicular to the substrate, here the intentional inclination of the substrate during deposition leads to a pronounced offset of 30° to the growth direction. In this case, “parallel” and “perpendicular” field orientations are particularly meaningless unless that is the actual direction in which the field is to be aligned in application. In the case of the ISD wire shown, I_c values parallel (0°) and perpendicular (90°) to the wire may be similar since they both lie between the minimum (30°) and maximum (120°) values. However, such an offset in the orientation of the peak I_c of the wires could make them highly beneficial if employed as the end turns in a hybrid coil structure as just described.

In-Plane Field Angle Variation

It is the observation at 77 K [48], and has been assumed to be true under all conditions, that the angular variation in I_c obtained for fields applied *within the plane* of the superconductor follows a simple geometric behaviour that sees it pass from some maximum value (limited by flux-line cutting or other effects) in the Lorentz force-free configuration of field and current parallel to a minimum value (under which most characterisation measurements are typically conducted) when the applied field and transport current are perpendicular, generating the maximum Lorentz force on the vortices which causes them to overcome their pinning.

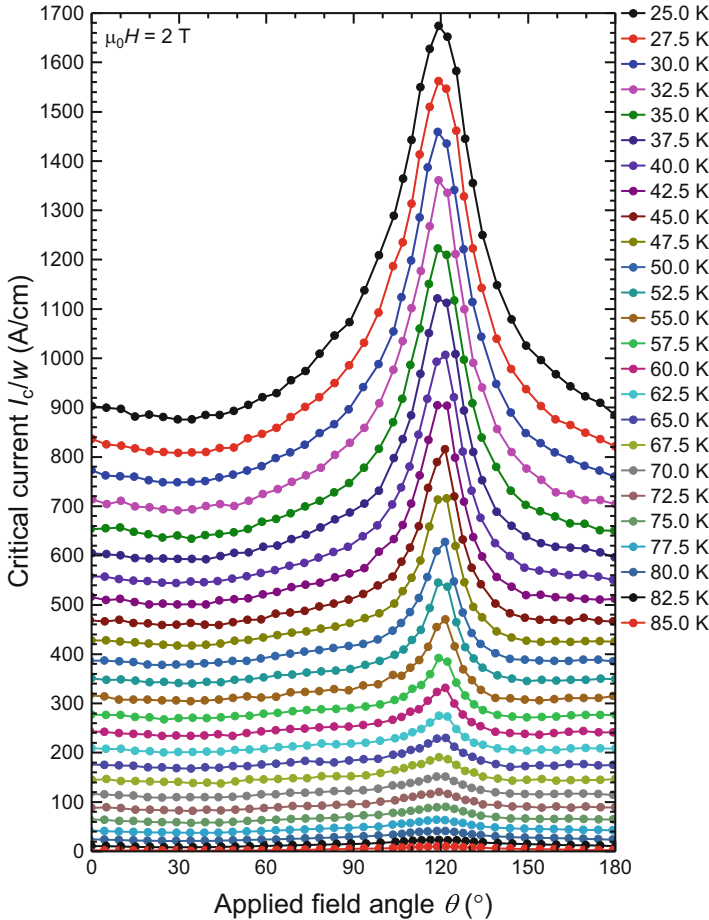


Fig. 1.12 Angle dependence of the critical current of an inclined substrate deposited 2G HTS wire sample from THEVA over a range of temperatures (lowest temperature corresponding to highest I_c) at an applied field of 2 T. The in-plane peak in I_c is shifted by 30° from 90° to 120° , reflecting the offset in the crystallographic orientation of the substrate. Data from [47]

However, it has been observed (Fig. 1.13) that this is not universally the case and that in particular at low temperatures and high fields, this typical behaviour can fully invert. I_c values as much as one third reduced have been observed in the force-free configuration compared to the usually measured maximum Lorentz force configuration, hard to explain by any reasonable degree of sample mismounting. This is a concern for any application seeking to utilise HTS wires under these

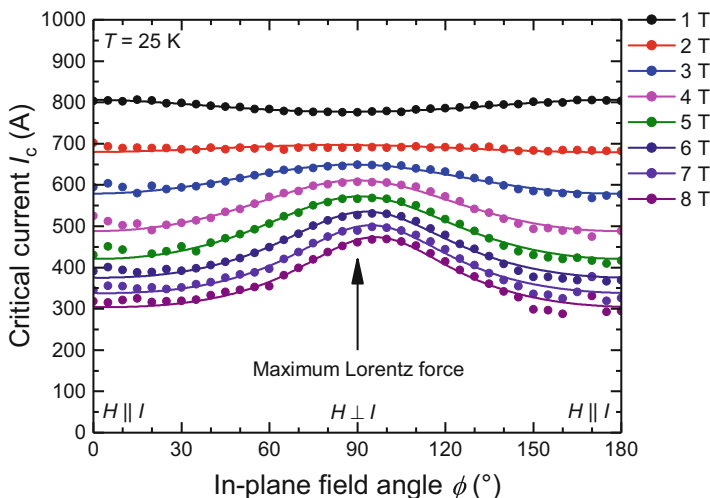


Fig. 1.13 In-plane angle dependence of the critical current of an American Superconductor 2G HTS wire sample, showing that at low temperature, high field, I_c values as much as 30% lower are obtained in the force-free configuration of field and current parallel (0°) than in the commonly measured maximum Lorentz force configuration of field perpendicular to current (180°). After [49]

sorts of extreme conditions, since this source of potential I_c variation is not commonly considered, with the maximum Lorentz force geometry usually taken as representing a worst case I_c .

Case Study: MRI Magnet

The coil design for a 3 T HTS MRI magnet is shown in Fig. 1.14. The design requirement is for the coil pack to generate a field of 3 T across a 6 cm diameter spherical volume at the centre of the bore, suitable for pre-clinical or extremity imaging. This requirement together with the proposed coil layout (optimised for field homogeneity, etc.) dictates the current required in the superconducting windings. In addition to calculating the resulting field within the bore of the magnet, the corresponding field distribution within the windings themselves can also be determined by finite element modelling, and it is this that is shown in terms of the colour map on the left panel of the figure indicating the local field strength and the field lines on the central panel indicating the local field orientation.

(continued)

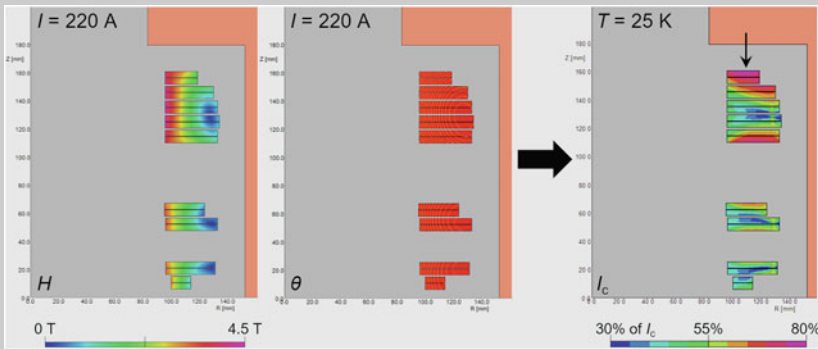


Fig. 1.14 Coil design of a 3 T HTS MRI magnet [12]. The magnet is rotationally symmetric about an axis along the left side of the image, and only the upper half of the symmetric magnet is shown, with the centre of the imaging volume at the bottom left corner of the image. The entire magnet comprises 18 double-pancake coils (9 shown) of varying internal and external radius designed to produce a homogeneous field region across a 6 cm diameter spherical volume at the centre of the bore when energised to 220 A. The left panel shows the field strength mapped across the coils, while the centre panel shows the field orientation at each point within the coils. Together with the detailed wire characterisation $I_c(T, B, \theta)$, these combine to produce the map shown on the right panel of the current at each point in the coils expressed as a fraction of the local I_c under those precise field conditions, for a given operating temperature chosen to yield the desired operating current margin. The critical region of the coil (closest to I_c) is indicated by an arrow

On the basis of this local field profile (strength and orientation) at each point in the conductor, it is possible to index these values with the local critical current under these exact field conditions and a given operating temperature, as determined by the detailed wire characterisation, and thereby to produce a plot showing the current in the coil as a fraction of the wire I_c at each point. A suitable operating temperature can then be chosen such that the coil remains below an acceptable fraction of the wire I_c , for example 80% of I_c as results here for a chosen operating temperature of 25 K. Such a plot is shown on the right panel of the figure, and a number of quite general observations can be made on the basis of this example.

First, the critical region of the coil (where the current most closely approaches I_c) is at neither the point of highest field strength (4.3 T on the innermost edge of the upper coil pack) nor the point of least favourable field orientation (field closely perpendicular to the tape) but rather it is located in the region of the coil where these two factors combine to produce the least favourable overall operating condition. This further highlights the potential advantages to be gained from a hybrid magnet design, as discussed in section “Wire Asymmetry”, using superior wire in the coils forming these

(continued)

critical regions, while utilising lower performance wire in less critical regions, many of which fall below 50% of I_c .

At this critical point in the coil, the precise field condition is a field strength of 2.8 T at an angle of 52° to the normal to the wire. Designing conservatively for a minimum I_c condition at 3 T would have resulted in a current limit of 240 A, which when derated to 80% of I_c would have limited the operating current to 190 A, requiring correspondingly more wire throughout the magnet in order to achieve the target field. Instead, utilising the full angle dependent wire characterisation allowed use of the full available wire performance, recognising its true I_c under these conditions of 280 A, 15% higher than the minimum value.

By utilising the full wire characterisation dataset at the design stage, the magnet design can be optimised to use the minimum amount of wire necessary to maintain the desired safety margin, greatly impacting on the overall cost of the magnet. Alternatively, detailed modelling on the basis of known wire performance can be used to safely raise the permissible operating temperature of a constructed magnet, allowing for longer periods of image acquisition, or greater intervals between cryocooler maintenance [23].

1.4 n -Value

An increasingly important engineering property of high-temperature superconductors is the n -value, or the exponent of the IV curve, which is typically lower (the curve is closer to linear) than its counterpart in the low-temperature superconductors (LTS). Microscopically, the n -value is determined by the form of the pinning potential, and thereby reflects the creep rate of flux within the superconductor [50], a thermally activated process of consequently greater significance in HTS than LTS [51]. It has a role to play in the operation of novel superconducting devices such as SQUIDS and flux pumps [52], magnet stability, quench behaviour, ramping rate, AC loss [53], etc. Unlike I_c , the n -value as determined from transport measurements is a poorly defined property since it relies on an assumed functional form of the IV curve, not merely the point at which it crosses a predefined value. This functional form is usually taken to be a power law although this is not an entirely accurate representation since actual experimental data deviates in both directions, below I_c where the data vanishes below the noise level and above I_c where heating effects or the transition to the flux flow regime cause a variation in the observed behaviour (in opposing senses). The power law is thus only an approximation to the functional form of the observed data in the vicinity of I_c . The I_c and n parameters of the IV curve fitting function are also highly interdependent, and Fig. 1.15 shows

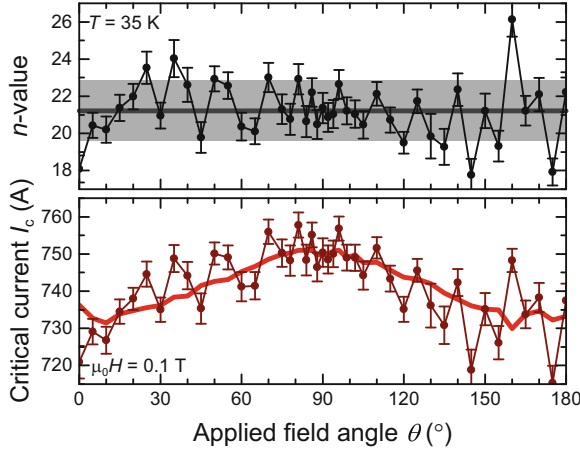


Fig. 1.15 Typical IV -curve fitting results for I_c and n (data points), highlighting the strong correlation between errors in the two fitting parameters due to their high interdependency. By smoothing the variation in n (in this case by simply fixing it at the average value across the curve), an improvement in the fidelity of the angular variation in I_c is simultaneously obtained (thick lines). The resulting fitting error in I_c in this case is indicated by the thickness of the line

how constraining (or smoothing) n can lead to a corresponding improvement in the determination of I_c . Modern measurement systems offer increased fidelity of n -value measurement in addition to I_c as exemplified in Fig. 1.16. Complex behaviours are seen to emerge and evolve across the measurement parameter space covering wide ranges of exponents from values as low as 5 at moderate fields, more commonly associated with 1G conductor materials, to values as high as 28 at zero field, approaching those of LTS [55].

At the higher fields shown, the simple variation in n -value with applied field angle featuring a cusp-like peak around 90° could easily be supposed to reflect a correlation with the typical form of the angle dependence of I_c of an anisotropic superconductor [54]. However, the I_c data of this particular pinning-enhanced wire (Fig. 1.11) bears no resemblance to this simple form, having a much narrower in-plane peak, and a broader and stronger out-of-plane peak resulting from the artificial pinning that is not at all reflected in the n -value data. Comparison with the data presented in [21] shows a similar evolution of behaviour towards lower fields, with a gradual flattening (isotropisation) of the curve towards 1 T, followed by the emergence of a broad 180° peak and steady growth of a sharp 90° peak, and then the re-emergence of a smoothly geometrical variation peaking around 90° , while the n -value steadily increases with reducing field, as is usually observed [56].

An often overlooked consequence of this systematic, uncorrelated, non-monotonic variation in n -value for pinning-enhanced samples, highlighted in [22], is that the *form* of the angular dependence of I_c can be made to vary depending on the particular arbitrary criterion chosen to define I_c , as shown in Fig. 1.17. This is incompatible with attempts to attribute this functional form directly to

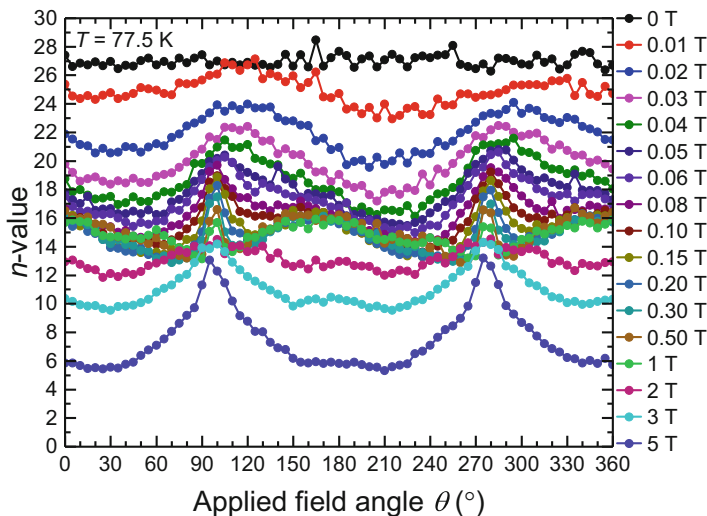


Fig. 1.16 Angle dependence of the n -value of the SuperPower AP 2G HTS wire sample for which the I_c data is shown in Fig. 1.11. A clear, systematic variation in n with both field and field angle is observed across the dataset. The curves converge between 0.1 T and 1 T, but deviate either side of this field range to values as high as 28 at 0 T and as low as 5 at 5 T

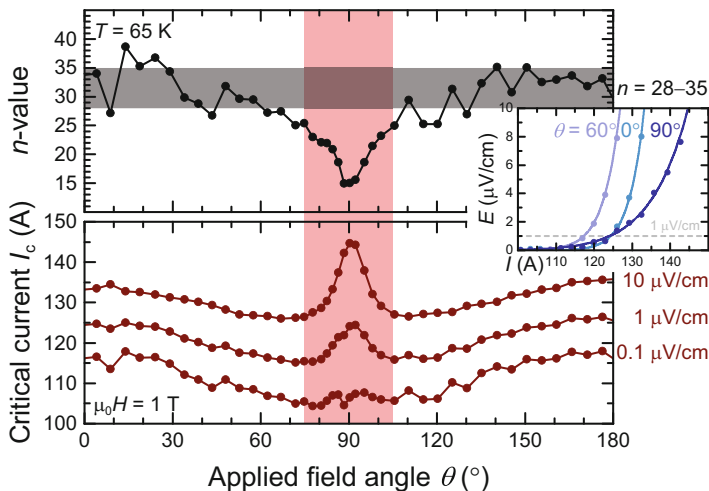


Fig. 1.17 Effect of a varying n -value (upper panel) on the perceived variation in I_c (lower panel) under different commonly employed electric field criteria used to define I_c . In this case, there is no doubt from the form of the IV curves (inset) that the variation in n -value is real making the definition of I_c in terms of a fixed arbitrary electric field criterion problematic. Data from the sample shown in Fig. 1.10. After [22]

microstructural pinning properties of the material [57] and indicates that a deeper understanding is required of the influences governing the variation in n -value with field angle in particular, and to the proper separation of the I_c and n parameters of the IV curve. Since there can be no doubt that the shape of the underlying IV curves does indeed vary, attempts to define a more fundamental measure of I_c may be required [58, 59].

1.5 Mechanical Strength

An aspect of wire characterisation that commonly takes second place to considerations of electrical performance, but which becomes critical at the point of device construction, is the mechanical strength of the wires. For 2G wires in particular, the point at which they fail due to delamination of the superconducting layer from the supporting substrate is critical, typically leading to imminent localised failure and burn-out.

A range of different methods exist for characterising this “delamination strength,” and it is important on comparing different results to be aware of what has actually been measured in each case. The mode I interfacial fracture energy (G_{IC}), as measured in a climbing drum peel test [60], is a well-defined physical property of a composite material considered to accurately reflect the parameter of importance to this application. Under a survey of high-quality production wire inserts (with only thin silver stabiliser) that have been demonstrated to be robust in use, this parameter is found to be remarkably consistent at around 5 J/m^2 , with interfacial failure eventually occurring within the buffer stack. Counterintuitively, a greater interfacial toughness is measured for those wires incorporating softer substrate materials such as stainless steel (rather than Hastelloy) or even better the Ni–W alloy used in the RABiTS process. This is explained as being due to deformation of the substrate absorbing some of the interfacial strain and thereby enabling the composite to survive intact to higher stresses.

Similarly, it is possible to positively influence the interfacial toughness by plating the HTS layer on the upper side with the usual copper electrical stabilisation layer, absorbing strain on that side of the conductor. Recent results (Mataira, private communication, 2018) starting from the same wire and applying successively thicker electroplated copper layers have indicated that it is possible to vary the resulting interfacial toughness of the wire over a wide range, extending up to at least 15 J/m^2 for plating thicknesses in excess of $100 \mu\text{m}$. Thus, it appears that any desired interfacial strength can be tailored from any given wire (of sufficient robustness), and so wire selection on the basis of electrical performance can proceed independently of strength considerations.

1.6 Targeted Wire Selection for Specific Applications

At the present time, many potentially beneficial applications of HTS technology are cost-limited. We find ourselves in the situation, common to many fledgling industries, where for the cost of the HTS wire to come down, the volume of demand must go up, but for demand to increase, the costs must come down.

By applying an improved understanding of the detailed properties of contemporary HTS wires, and thereby avoiding the excessive over-engineering of devices that results from a generalised or limited understanding of specific wire performance under conditions relevant to the target application, a significant reduction in the quantity of wire required for a particular device can be realised, with no reduction in device performance or reliability, and in many cases with a simultaneous improvement. With wire cost presently the major portion of the total device cost in many instances, this saving directly carries through to the final device cost. In this way, the arguments for the benefits of HTS-based technologies can be enhanced on an economic basis, where they often fall short.

While wire development continues apace, it is inevitable that targeted wire characterisation will be a necessary prerequisite for any large new project in order to achieve the above. In time, however, it is to be hoped that wire manufacturers will be in a position to fully specify their product, and that informed selection of the most appropriate wire for a given application will become possible on the basis of manufacturer specifications.

Acknowledgements The author gratefully acknowledges the significant contribution of his colleague Nicholas M. Strickland to the work summarised here.

References

1. P. Tixador, Development of superconducting power devices in Europe. *Phys. C* **470**, 971 (2010)
2. B. Gamble, G. Snitchler, T. MacDonald, Full power test of a 36.5 MW HTS propulsion motor. *IEEE Trans. Appl. Supercond.* **21**, 1083 (2011)
3. A. Hobl, W. Goldacker, B. Dutoit, L. Martini, A. Petermann, P. Tixador, Design and production of the ECCOFLOW resistive fault current limiter. *IEEE Trans. Appl. Supercond.* **23**, 5601804 (2013)
4. M. Stemmler, F. Merschel, M. Noe, A. Hobl, AmpaCity — advanced superconducting medium voltage system for urban area power supply, in *2014 IEEE PES T&D Conf. Expo* (2014). <https://doi.org/10.1109/TDC.2014.6863566>
5. G.G. Sotelo, R.A.H. de Oliveira, F.S. Costa, D.H.N. Dias, R. de Andrade, R.M. Stephan, A full scale superconducting magnetic levitation (MagLev) vehicle operational line. *IEEE Trans. Appl. Supercond.* **25**, 3601005 (2015)
6. R. Gupta, M. Anerella, P. Joshi, J. Higgins, S. Lalitha, W. Sampson, J. Schmalzle, P. Wanderer, Design, construction, and testing of a large-aperture high-field HTS SMES coil. *IEEE Trans. Appl. Supercond.* **26**, 5700208 (2016)

7. S. Mukoyama, K. Nakao, H. Sakamoto, T. Matsuoka, K. Nagashima, M. Ogata, T. Yamashita, Y. Miyazaki, K. Miyazaki, T. Maeda, H. Shimizu, Development of superconducting magnetic bearing for 300 kW flywheel energy storage system. *IEEE Trans. Appl. Supercond.* **27**, 3600804 (2017)
8. N. Glasson, M. Staines, N. Allpress, M. Pannu, J. Tanchon, E. Pardo, R. Badcock, R. Buckley, Test results and conclusions from a 1 MVA superconducting transformer featuring 2G HTS Roebel cable. *IEEE Trans. Appl. Supercond.* **27**, 5500205 (2017)
9. J. Kellers, Development of a superconductive wind power generator within the EcoSwing project. Presented at the 25th International Conference on Magnet Technology, Amsterdam (2017)
10. D.M. Pooke, V. Chamritski, M. Fee, S. Gibson, B.T. King, J.L. Tallon, M. Meissner, R. Feyerherm, S.R. Olsen, S.J. Kennedy, R.A. Robinson, HTS 5 tesla synchrotron and neutron beamline magnets. *IEEE Trans. Appl. Supercond.* **19**, 1372 (2009)
11. S. Yoon, J. Kim, K. Cheon, H. Lee, S. Hahn, S.-H. Moon, 26 T 35 mm all-GdBa₂Cu₃O_{7-x} multi-width no-insulation superconducting magnet. *Supercond. Sci. Technol.* **29**, 04LT04 (2016)
12. B.J. Parkinson, K. Bouloukakakis, R.A. Slade, A compact 3 T all HTS cryogen-free MRI system. *Supercond. Sci. Technol.* **30**, 125009 (2017)
13. M.V. Silva Elipe, N. Donovan, R. Krull, D. Pooke, K.L. Colson, Performance of new 400-MHz HTS power-driven magnet NMR technology on typical pharmaceutical API, cinacalcet HCl. *Magn. Reson. Chem.* **56**, 817 (2018)
14. B.N. Sorbom, J. Ball, T.R. Palmer, F.J. Mangiarotti, J.M. Sierchio, P. Bonoli, C. Kasten, D.A. Sutherland, H.S. Barnard, C.B. Haakonsen, J. Goh, C. Sung, D.G. Whyte, ARC: a compact, high-field, fusion nuclear science facility and demonstration power plant with demountable magnets. *Fusion Eng. Des.* **100**, 378 (2015)
15. A. Sykes, A.E. Costley, C.G. Windsor, O. Asunta, G. Brittles, P. Buxton, V. Chuyanov, J.W. Connor, M.P. Gryaznevich, B. Huang, J. Hugill, A. Kukushkin, D. Kingham, A.V. Langtry, S. McNamara, J.G. Morgan, P. Noonan, J.S.H. Ross, V. Shevchenko, R. Slade, G. Smith, Compact fusion energy based on the spherical tokamak. *Nucl. Fusion* **58**, 016039 (2017)
16. P.M. Leys, M. Klaeser, F. Schleissinger, T. Schneider, Angle-dependent $U(I)$ measurements of HTS coated conductors. *IEEE Trans. Appl. Supercond.* **23**, 8000604 (2013)
17. K. Tsuchiya, A. Kikuchi, A. Terashima, K. Suzuki, K. Norimoto, M. Tawada, M. Masuzawa, N. Ohuchi, X. Wang, Y. Iijima, T. Takao, S. Fujita, M. Daibo, Y. Iijima, Critical current characterization of commercial REBCO coated conductors at 4.2 and 77 K. *IEEE Trans. Appl. Supercond.* **27**, 6600205 (2017)
18. P. Sunwong, J.S. Higgins, D.P. Hampshire, Probes for investigating the effect of magnetic field, field orientation, temperature and strain on the critical current density of anisotropic high-temperature superconducting tapes in a split-pair 15 T horizontal magnet. *Rev. Sci. Instrum.* **85**, 065111 (2014)
19. H. Ma, H. Liu, F. Liu, H. Zhang, L. Ci, Y. Shi, L. Lei, Critical current measurements of high-temperature superconducting short samples at a wide range of temperatures and magnetic fields. *Rev. Sci. Instrum.* **89**, 015102 (2018)
20. C. Barth, M. Bonura, C. Senatore, High current probe for $I_c(B, T)$ measurements with ± 0.01 K precision: HTS current leads and active temperature stabilization system. *IEEE Trans. Appl. Supercond.* **28**, 9500206 (2018)
21. M. Lao, J. Hänisch, S. Kauffmann-Weiss, R. Gehring, H. Fillinger, A. Drechsler, B. Holzpfafel, High current variable temperature electrical characterization system for superconducting wires and tapes with continuous sample rotation in a split coil magnet. *Rev. Sci. Instrum.* **90**, 015106 (2019)
22. N.M. Strickland, C. Hoffmann, S.C. Wimbush, A 1 kA-class cryogen-free critical current characterization system for superconducting coated conductors. *Rev. Sci. Instrum.* **85**, 113907 (2014)
23. S.C. Wimbush, N.M. Strickland, A public database of high-temperature superconductor critical current data. *IEEE Trans. Appl. Supercond.* **27**, 8000105 (2017)

24. V. Selvamanickam, Y. Yao, Y. Chen, T. Shi, Y. Liu, N.D. Khatri, J. Liu, C. Lei, E. Galstyan, G. Majkic, The low-temperature, high-magnetic-field critical current characteristics of Zr-added (Gd, Y)Ba₂Cu₃O_x superconducting tapes. *Supercond. Sci. Technol.* **25**, 125013 (2012)
25. A. Xu, L. Delgado, M. Heydari Gharahcheshmeh, N. Khatri, Y. Liu, V. Selvamanickam, Strong correlation between $J_c(T, H||c)$ and $J_c(77K, 3T||c)$ in Zr-added (Gd, Y)BaCuO coated conductors at temperatures from 77 down to 20 K and fields up to 9 T. *Supercond. Sci. Technol.* **28**, 082001 (2015)
26. S. Awaji, M. Namba, K. Watanabe, H. Kai, M. Mukaida, S. Okayasu, Flux pinning properties of correlated pinning at low temperatures in ErBCO films with inclined columnar defects. *J. Appl. Phys.* **111**, 013914 (2012)
27. N.M. Strickland, S.C. Wimbush, J.V. Kennedy, M.C. Ridgway, E.F. Talantsev, N.J. Long, Effective low-temperature flux pinning by Au ion irradiation in HTS coated conductors. *IEEE Trans. Appl. Supercond.* **25**, 6600905 (2015)
28. M.W. Rupich, S. Sathyamurthy, S. Fleshler, Q. Li, V. Solovyov, T. Ozaki, U. Welp, W.-K. Kwok, M. Leroux, A.E. Koshelev, D.J. Miller, K. Kihlstrom, L. Civale, S. Eley, A. Kayani, Engineered pinning landscapes for enhanced 2G coil wire. *IEEE Trans. Appl. Supercond.* **26**, 6601904 (2016)
29. S.C. Wimbush, N.M. Strickland, Critical current characterisation of SuperOx 2G HTS superconducting wire, figshare (2016), <https://doi.org/10.6084/m9.figshare.3759315.v1>
30. Sumitomo Electric Industries, Ltd., *Sumitomo BSCCO Wire (DI-BSCCO) Type H Specifications* (2018). Available at: https://global-sei.com/super/hts_e/type_h.html. Accessed 30 Nov 2018
31. S.C. Wimbush, N.M. Strickland, N.J. Long, Low-temperature scaling of the critical current in 1G HTS wires. *IEEE Trans. Appl. Supercond.* **25**, 6400105 (2015)
32. N.M. Strickland, S.C. Wimbush, The magnetic-field dependence of critical current: what we really need to know. *IEEE Trans. Appl. Supercond.* **27**, 8000505 (2017)
33. D.T. Verebelyi, D.K. Christen, R. Feenstra, C. Cantoni, A. Goyal, D.F. Lee, M. Paranthaman, P.N. Arendt, R.F. DePaula, J.R. Groves, C. Prouteau, Low angle grain boundary transport in YBa₂Cu₃O_{7- δ} coated conductors. *Appl. Phys. Lett.* **76**, 1755 (2000)
34. K.-H. Müller, D.N. Matthews, A model for the hysteretic critical current density in polycrystalline high-temperature superconductors. *Phys. C* **206**, 275 (1993)
35. M. Däumling, E. Sarnelli, P. Chaudhari, A. Gupta, J. Lacey, Critical current of a high T_c Josephson grain boundary junction in high magnetic field. *Appl. Phys. Lett.* **61**, 1355 (1992)
36. A.A. Gapud, D.K. Christen, R. Feenstra, F.A. List III, A. Khan, On narrowing coated conductor film: the emergence of granularity-induced field hysteresis of transport critical current. *Supercond. Sci. Technol.* **21**, 075016 (2008)
37. Y. Nakagawa, Y. Mawatari, H. Yamasaki, M. Murugesan, K. Develos-Bagarinao, Angular hysteresis in the critical current density of laser-patterned REBa₂Cu₃O_y films. *IEEE Trans. Appl. Supercond.* **17**, 3597 (2007)
38. S.A. Harrington, J.L. MacManus-Driscoll, J.H. Durrell, Practical vortex diodes from pinning enhanced YBa₂Cu₃O_{7- δ} . *Appl. Phys. Lett.* **95**, 022518 (2009)
39. N.M. Strickland, S.C. Wimbush, M.W. Rupich, N.J. Long, Asymmetries in the field and angle dependences of the critical current in HTS tapes. *IEEE Trans. Appl. Supercond.* **29**, 8001304 (2019)
40. F. Gömöry, J. Šouc, E. Seiler, M. Vojenčiak, X. Granados, Modification of critical current in HTSC tape conductors by a ferromagnetic layer. *J. Phys.: Conf. Ser.* **97**, 012096 (2008)
41. H.-J. Sung, B.-S. Go, H. Park, R.A. Badcock, M. Park, I.-K. Yu, Design, fabrication, and analysis of HTS coils for a 10-kW wind power generator employing a brushless exciter. *IEEE Trans. Appl. Supercond.* **27**, 5202305 (2017)
42. C.W. Bumby, R.A. Badcock, H.-J. Sung, K.-M. Kim, Z. Jiang, A.E. Pantoja, P. Bernardo, M. Park, R.G. Buckley, Development of a brushless HTS exciter for a 10 kW HTS synchronous generator. *Supercond. Sci. Technol.* **29**, 024008 (2016)
43. S.C. Wimbush, N.M. Strickland, Critical current characterisation of AMSC Amperium 2G HTS superconducting wire, figshare (2014), <https://doi.org/10.1063/1.4902139>

44. Z. Jiang, N.J. Long, M. Staines, R.A. Badcock, C.W. Bumby, R.G. Buckley, N. Amemiya, AC loss measurements in HTS coil assemblies with hybrid coil structures. *Supercond. Sci. Technol.* **29**, 095011 (2016)
45. Z. Jiang, N. Endo, S.C. Wimbush, J. Brooks, W. Song, D. Miyagi, M. Tsuda, Exploiting asymmetric wire critical current for the reduction of AC loss in HTS coil windings. *Supercond. Sci. Technol.* submitted (2019)
46. W. Prusseit, G. Sigl, R. Nemetschek, C. Hoffmann, J. Handke, A. Lümke, H. Kinder, Commercial coated conductor fabrication based on inclined substrate deposition. *IEEE Trans. Appl. Supercond.* **15**, 2608 (2005)
47. S.C. Wimbush, N.M. Strickland, Critical current characterisation of THEVA pre-production 2G HTS superconducting wire, figshare (2016), <https://doi.org/10.6084/m9.figshare.3759327.v1>
48. J.R. Clem, M. Weigand, J.H. Durrell, A.M. Campbell, Theory and experiment testing flux-line cutting physics. *Supercond. Sci. Technol.* **24**, 062002 (2011).
49. S.C. Wimbush, N.M. Strickland, N.J. Long, In-plane field angle dependence of the critical current of RBCO wires at low temperatures. *Phys. Proc.* **81**, 81 (2016)
50. L. Opherden, M. Sieger, P. Pahlke, R. Hühne, L. Schultz, A. Meledin, G. Van Tendeloo, R. Nast, B. Holzapfel, M. Bianchetti, J. L. MacManus-Driscoll, J. Hänisch, Large pinning forces and matching effects in $\text{YBa}_2\text{Cu}_3\text{O}_{7-\delta}$ thin films with $\text{Ba}_2\text{Y}(\text{Nb}/\text{Ta})\text{O}_6$ nano-precipitates. *Sci. Rep.* **6**, 21188 (2016)
51. M. Chudy, Z. Zhong, M. Eisterer, T. Coombs, n -values of commercial YBCO tapes before and after irradiation by fast neutrons. *Supercond. Sci. Technol.* **28**, 035008 (2015)
52. M.D. Ainslie, C.W. Bumby, Z. Jiang, R. Toyomoto, N. Amemiya, Numerical modelling of dynamic resistance in high-temperature superconducting coated-conductor wires. *Supercond. Sci. Technol.* **31**, 074003 (2018)
53. N. Amemiya, K. Miyamoto, N. Banno, O. Tsukamoto, Numerical analysis of AC losses in high T_c superconductors based on $E - j$ characteristics represented with n -value. *IEEE Trans. Appl. Supercond.* **7**, 2110 (1997)
54. S. Oh, H. Choi, C. Lee, S. Lee, J. Yoo, D. Youm, H. Yamada, H. Yamasaki, Relation between the critical current and the n value of ReBCO thin films: a scaling law for flux pinning of ReBCO thin films. *J. Appl. Phys.* **102**, 043904 (2007)
55. D.M.J. Taylor, D.P. Hampshire, Relationship between the n -value and critical current in Nb_3Sn superconducting wires exhibiting intrinsic and extrinsic behaviour. *Supercond. Sci. Technol.* **18**, S297 (2005)
56. B. Dutoit, M. Sjöström, S. Stavrev, Bi(2223) Ag sheathed tape I_c and exponent n characterization and modelling under DC applied magnetic field. *IEEE Trans. Appl. Supercond.* **9**, 809 (1999)
57. S.C. Wimbush, N.J. Long, The interpretation of the field angle dependence of the critical current in defect-engineered superconductors. *New J. Phys.* **14**, 083017 (2012)
58. E.F. Talantsev, N.M. Strickland, S.C. Wimbush, W.P. Crump, The onset of dissipation in high-temperature superconductors: self-field experiments. *AIP Adv.* **7**, 125230 (2017)
59. E.F. Talantsev, N.M. Strickland, S.C. Wimbush, J. Brooks, A.E. Pantoja, R.A. Badcock, J.G. Storey, J.L. Tallon, The onset of dissipation in high-temperature superconductors: magnetic hysteresis and field dependence. *Sci. Rep.* **8**, 14463 (2018)
60. N.J. Long, R.C. Maitra, E. Talantsev, R.A. Badcock, Mode I delamination testing of REBCO coated conductors via climbing drum peel test. *IEEE Trans. Appl. Supercond.* **28**, 6600705 (2018)